Kinetics and thermodynamics of acoustic release of doxorubicin from non-stabilized polymeric micelles

Ghaleb A. Husseini[a,*], Dana Stevenson-Abouelnasr[a], William G. Pitt[b], Khaled T. Assaleh[c], Lujein O. Farahat[a], Jalal Fahadi[a]

[a] Chemical Engineering Department, American University of Sharjah, Sharjah, United Arab Emirates [b] Department of Chemical Engineering, Brigham Young University, Provo, Utah 84602, United Arab Emirates [c] Electrical Engineering Department, American University of Sharjah, Sharjah, United Arab Emirates

https://doi.org/10.1016/j.colsurfa.2010.01.044

This paper studies the thermodynamic characteristics of ultrasound-activated release of Doxorubicin (Dox) from micelles. The release and re-encapsulation of Dox into Pluronic® P105 micelles was measured by recording the fluorescence of a solution of 10g/ml Dox and 10wt% P105 polymer in phosphate buffered saline, during and after insonation by ultrasound at three temperatures (25◦C, 37◦C and 56◦C). The experimental data were modeled using a previously published model of the kinetics of the system. The model was simplified by the experimental measurement of one of the parameters, the maximum amount of Dox that can be loaded into the poly(propyleneoxide) cores of the micelles, which was found to be 89mg/ml PPO and 150mg Dox/ml PPO at 25◦C and 37◦C, respectively. From the kinetic constants and drug distribution parameters, we deduced the thermodynamic activation energy for micelle re-assembly and the residual activation energies for micelle destruction. Our model showed that the residual activation energy for destruction decreased with increasing acoustic intensity. In addition, higher temperatures were found to encourage micelle destruction and hinder micelle re-assembly.

1. Introduction

Therapeutic ultrasound (US) has recently been applied for the site-specific delivery of drugs and genetic material. The advantages of US-activated drug and gene delivery include the ability to focus ultrasound on a target tissue [1], the ability to both visualize the tumor and activate the release with the same instrument [2,3], and perhaps most importantly the minimal stress to the patient because there is no surgery or pain associated with the transdermal delivery of acoustic energy. Although US can be used to deliver heat for hyperthermic therapy, most applications that involve drug or gene delivery are done at relatively low intensities and with a minimal deposition of thermal energy. Instead, the therapy relies on non-thermal "mechanical effects", such as radiation pressure and bubble cavitation[1,4].In brief, radiation pressure is a phenomenon in which acoustic pressure is used to push bubbles, liposomes or emulsions within a tissue, such as pushing microbubbles against the side of a blood vessel [5,6]. Cavitation is the formation and oscillation of bubbles within a fluid medium. Ultrasound can excite these bubbles sufficiently to enhance convection and shear stress near the bubble, or to cause bubble collapse and destruction. The latter has been correlated with the delivery of drugs and genes to cells [1,4,7–16].

The targeted delivery of material using ultrasound has been reported for both in vitro and in vivo systems. Our group has been investigating the use of ultrasound to release Doxorubicin (Dox) from polymeric micelles to cancerous tissue in vitro [8,17–22] and in vivo [23–25]. We and others have shown that US is able to release chemotherapy drugs from the cores of the micelles in therapeutically significant amounts [17,18,26,27]. Hosseinkhani and Tabata's research group has similarly shown that ultrasound can be used successfully in gene delivery [28–35]. Our work showed that the amount of drug release increases as the acoustic intensity is increased or as the frequency is decreased [8,18,22].

In a previous publication, we reported the results of a novel kinetic model involving US and bubble cavitation that was capable of representing the kinetics of Dox release from unstabilized Pluronic® P105 micelles under ultrasonic stimulus [36]. The model attempted to capture drug-release kinetics and involved several parameters such as rates of micelle destruction, micelle assembly, drug re-encapsulation, nuclei destruction, and the maximal loading of Dox in micelles.

The transient release and re-encapsulation are processes in which concentration gradients and possibly some fluid convection operate to transport the drugs from the carrier to the

cell cytosol. These are non-equilibrium phenomena. As such, it is informative and beneficial (in the aspect of drug carrier design) to obtain or derive information related to these processes. For example, it would be useful to know the partition coefficient or the equilibrium distribution of drug between the interior of the micellar carrier and the surrounding aqueous environment. Such data would aid in designing formulations and estimating the expected amount of drug release. Although there is an abundance of mathematical models describing ultrasonic cavitation and destruction of microbubbles [37–42] and liposomes [43–50], there are very few models describing the perturbation of micelles and the associated release of drug.

Herein we use of the above-mentioned drug-release model to represent the acoustic release and re-encapsulation kinetics of Pluronic® P105 micelles at various power densities and temperatures. Then we use the calculated kinetic constants at different temperatures to deduce some thermodynamics parameters relating to micellar destruction, re-assembly and re-encapsulation, including values of the activation and residual activation energies of ultrasonic-induced drug release from micelles.

2. Materials and methods

2.1. Drug encapsulation in Pluronic® unstabilized/stabilized micelles

Stock solutions of Pluronic® P105 (gift from BASF, Mount Olive, NJ) were prepared by dissolving the polymer in a PBS (phosphate buffered saline) solution to a final concentration of 10wt%. Dox (Pharmacia & Upjohn Company Kalamazoo MI) in dosage form (1:5, Dox:lactose) was dissolved into the P105 solutions at room temperature to produce a final Dox concentration of 10g/ml in 10wt% Pluronic®. As a control, the same drug concentration was also prepared in PBS [8,22].

2.2. Measuring ultrasound-triggered release of Dox from Pluronic® P105 micelles

The fluorescence properties of Dox are used to calculate the amount of its release from micelles. A custom ultrasonic exposure chamber with fluorescence detection was used to measure the release of Dox from Pluronic® micelles at three power intensities, at 70kHz, and three temperatures [22]. An argon-ion laser was directed into an acoustically transparent tube containing the micellar solution to be sonicated. As the drug molecules were excited at 488nm their fluorescence was collected using a coaxial fiber optic collector. The detector signal was digitized for computer storage and processing. It is well established that fluorescent drugs are able to fluoresce more in hydrophobic than in aqueous environments. Thus, Dox being an aromatic compound, it exhibits a decrease in fluorescence when it leaves the hydrophobic interior of the micelle to interact with surrounding water molecules. By measuring the fluorescence of Dox in PBS (baseline or 100% release) and in 10% Pluronic® solution (100% encapsulation or 0% release), one can calculate the amount of Dox released ultrasonically into water from the decrease in fluorescence. Ultrasound at 70kHz was generated in a Sonicor 100 bath (Copiague, NY). The intensity was controlled using a variac and monitored using a hydrophone (Bruel and Kjaer model 8103, Decatur, GA). During insonation, fluorescence decreased as expected. Ultrasound was manually turned on for 2s and then turned off for 2s. The fluorescence of eight cycles was recorded at each ultrasonic intensity. Although release experiments were conducted at 15 different power densities, in this paper we analyzed the data collected at the highest three acoustic intensities where the most significant release was observed. For more details refer to our previous article [8].

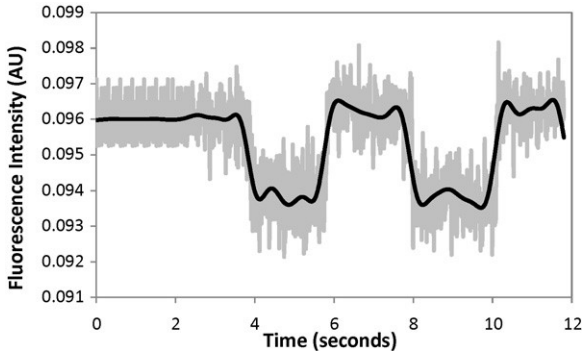

Fig. 1. Raw and filtered fluorescence data at 25◦C and 0.765W/cm^2 at 70kHz. Light gray points show raw data, and the solid black line shows the same data filtered using wavelets.

2.3. Data analysis

The raw fluorescence data exhibit large levels of high frequency noise. Hence, an efficient filtering (denoising) method is needed to remove this noise while preserving the important transitions that represents the rapid change in fluorescence. Conventional low pass filtering techniques do not offer a viable solution to this problem since the signal transitions will be severely blurred. As such, wavelet transform is well suited to the denoising of signals with sharp transients. A multi-level wavelet transformation is done to obtain the wavelet coefficients that represent the various frequency sub-bands of the signal. These coefficients are then thresholded to remove the high frequency noise and, at the same time, preserve the important transitions in

the signal. Fig. 1 shows the result of filtering the high frequency noise of the raw florescence data via wavelet denoising.

After wavelet denoising, the eight cycles were averaged for each temperature and acoustic intensity. The timing for each cycle was set at zero at the point of the initial rapid decrease in fluorescence. The eight cycles were overlayed and averaged from zero to 1.5s to provide the release portion of the data. Fig. 2a illustrates the preprocessing of fluorescence data at 56◦C and 0.675W/cm^2.

Since the pulsing of ultrasound was done manually, the cycle time was not precisely 2s. For this reason, there-encapsulation portion, occurring after the ultrasound is turned off, does not precisely coincide for all eight cycles. Instead, the eight cycles were over-layed a second time, to align the re-encapsulation portion, and averaged from 1.1 to 2.2s. This is illustrated for 56◦C and 0.675W/cm^2 in Fig. 2b. The final averaged signal for the entire 2-s cycle was obtained by averaging the release and re-encapsulation portions, including the overlapping section between 1.1 and 1.5s.

2.4. Measuring the amount of drug at saturation

The maximum amount of Dox which can be encapsulated in a 10% P105 solution, $^{E_{tot}^{sat}}{}_{,o}$, was estimated by first measuring the concentration of Dox for the entire solution at saturation, $[Dox]^{sat}$, which includes both the encapsulated drug and the drug dissolved in the PBS solution. This was accomplished by adding Dox in 2mg increments to a 10% P105 solution until a precipitate was observed. After every addition of the drug, the resulting solution was vortexed and observed for any drug settling at the bottom. In 2ml of 10% P105, 11.22mg of Dox dissolved before any precipitate was observed at 25◦C, while at 37◦C, it took 18.83mg of Dox to saturate 2ml of a 10% P105 micelle solution.

2.5. Encapsulation model

The amount of Dox which was encapsulated during and post insonation was simulated using a model previously described [36]. The model assumes that the diameters of micelles before insonation are normally distributed, with most micelles between 10 and 20nm in diameter. The normal distribution was divided into five groups, each comprising 20% of the total amount of polymer (Table 1). The simulation followed each group of micelles, allowing portions of each to be destroyed by insonation, reassemble, and re-encapsulate Dox. In our previous work, the value was unknown for $^{E_{tot}^{sat}}{}_{,o}$ the total amount of Dox that the intact micelles can hold. This required that it be a fitted parameter of the model. Unfortunately, $E_{tot}^{sat}{}_{,o}$ and (another model parameter) are closely coupled, creating difficulty in finding a unique solution to both. In this work, we use the magnitude of the experimental determination of $^{E_{tot}^{sat}}{}_{,o}$ to simplify the model. As will be shown in the results, $^{E_{tot}^{sat}}{}_{,o}$ is very large, such that the amount of Dox which could be encapsulated in micelle group j, E_j^{sat}, is large relative to the actual amount of Dox encapsulated in micelle group j, E_j. Therefore, E_j in Eq. (17) of our previous work may be neglected, and it simplifies to the following relation:

$$\left(\frac{dE_j}{dt}\right)_{encapsulation} = k_{e,j} F E_j^{sat} \quad (1)$$

Table 1
Characteristics for each micellar group.

Group (j)	Probability	Range (Z)	Diameter range (D, nm)[a]	Mean diameter ($\bar{D}_j$, nm)[a]	Mean cubed diameter ($\bar{D}_j^3$, nm^3)	Fraction of total micelles (M_j)
1	0.2	$-\infty \le Z < -0.84$	$0 \le D < 12.9$	11.6	1618	0.372
2	0.2	$-0.84 \le Z < -0.25$	$12.9 \le D < 14.4$	14.0	2670	0.226
3	0.2	$-0.25 \le Z < 0.25$	$14.4 \le D < 15.6$	15.0	3411	0.177
4	0.2	$0.25 \le Z < 0.84$	$15.6 \le D < 17.1$	16.5	4469	0.135
5	0.2	$0.84 \le Z < \infty$	$17.1 \le D < \infty$	19.6	6765	0.089

[a] These units were mistakenly listed as m in our previous publication [36].

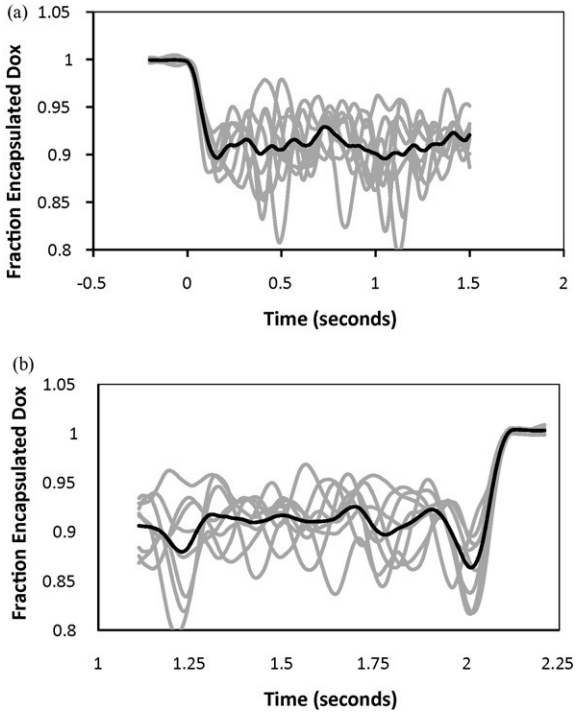

Fig. 2. A representative example of overlaying eight filtered ultrasound exposure cycles to determine the average for both the release segment ((a) ultrasound on at time=0) and the re-encapsulation segment ((b) ultrasound off at time=2s). Data are taken at 56C and 0.675W/cm^2.

The variable F is the amount of Dox that is free in the aqueous solution, and $k_{e,j}$ is a rate constant for the encapsulation of Dox. Eqs. (18) and (21) from the previous work [36] are substituted into Eq. (1).

$$\left(\frac{dE_j}{dt}\right)_{\text{encapsulation}} = \frac{\gamma}{\bar{D}_j} FnM_j \frac{\bar{D}_j^3}{\sum_{j=1}^{n} \bar{D}_j^3} E_{\text{tot,o}}^{\text{sat}} \quad (2)$$

D_j is the mean diameter for micelle group j, M_j is the number of micelles in group j, n is the number of micelle groups (5), and γ is a constant relating $k_{e,j}$ to micelle diameter. Finally, a single parameter for encapsulation is introduced, λ, which incorporates, γ, n, and $^{E_{tot}^{sat}}_{,o}$.

$$\left(\frac{dE_j}{dt}\right)_{\text{encapsulation}} = \lambda FM_j \frac{\bar{D}_j^3}{\bar{D}_j \sum_{j=1}^{n} \bar{D}_j^3} \quad (3)$$

The encapsulation term in Eq. (3) models only the forward reaction in a reversible system. That system includes both the encapsulation and the diffusive release of drug into and out of the micelle. The reverse reaction, diffusive release, will not be added to this model, as any fitted parameter for that reaction is closely coupled to the parameter of the forward reaction, Therefore, a unique solution to both parameters is not possible. Instead, will serve to model the effective encapsulation rate, defined as the forward minus the reverse reaction rate.

3. Results and discussion

3.1. Total micellar drug capacity

The total micellar drug capacity, $^{E_{tot}^{sat}}_{,o}$, was estimated from the experimental measure of $[Dox]^{sat}$. The overall amount of Dox dissolved at the saturation point is divided between two phases in the solution: (i) the hydrophobic core of each micelle, consisting of the poly-propylene oxide, PPO, portion of the Pluronic® molecules; and (ii) the PBS aqueous phase. A simple mass balance yields:

$$[Dox]^{sat} = [Dox]^{sat}_{PPO} V_{PPO} + [Dox]^{sat}_{PBS} V_{PBS} \quad (4)$$

The assumption that Dox is distributed between these two phases according to a constant partition coefficient, $P_{PPO/PBS}$, allows the substitution for $[Dox]^{sat}_{PBS}$ in the above equation, which can then be rearranged and solved for $[Dox]^{sat}_{PPO}$.

$$[Dox]^{sat}_{PPO} = \frac{[Dox]^{sat}}{V_{PPO} + (1/P_{PPO/PBS}(V_{PBS}))} \quad (5)$$

The partition coefficient for Dox in this drug delivery system is estimated to be at least 70 [51]. Thus, 70 molecules of Dox partition inside the PPO micelle core for every molecule present in the hydrophilic/aqueous phase (both water and free Pluronic® chains).

The volumes of PPO and PBS are estimated from the weight percent of each phase. Keeping in mind that the sonicated micellar solution had a final concentration of 10wt%Pluronic® and that P105 has the following structure: PEO_{37}-PPO_{56}-PEO_{37}, we calculate the

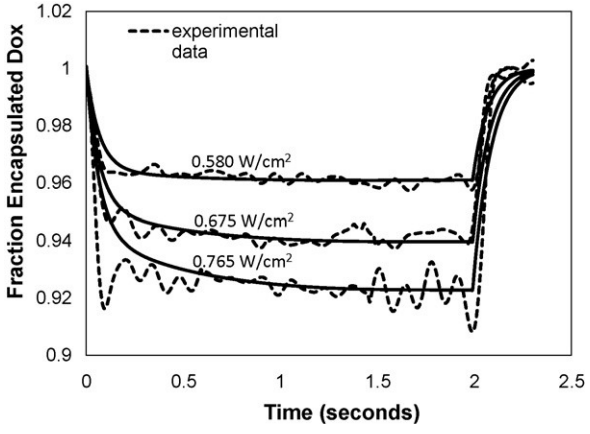

Fig. 3. Fluorescence data and model prediction at three different ultrasound intensities (0.580W/cm^2, 0.675W/cm^2 and 0.765W/cm^2) at 25◦C. Dotted line represents the average of 8 filtered runs. The solid line shows the fit of the model at the same temperature.

weight percent of PPO in pure P105 to be 49.94%. Thus the weight percent of PPO in our 10% P105 micellar solution is 4.994%, while the weight percent of PBS is 90%. Assuming a basis of 1ml of the 10% P105 micellar solution and that the specific gravity of the P105 copolymer is approximately 1, we have 0.04994ml of PPO (V_{PPO}) and 0.9ml of PBS (V_{PBS}).

Using the method described in the methods section, we measured the saturation limit of Dox in 10% P105 ($[Dox]^{sat}$) at 5.6083mg Dox/ml at 25◦C and 9.42mg Dox/ml at 37◦C. Substituting these values into Eq. (5) provides the estimate of 89mg Dox per ml PPO at saturation. The same calculation can be performed at 37◦C to yield a $[Dox]^{sat}_{PPO}$ = 150mg Dox/ml PPO. $^{E}_{tot}{}^{sat}_{,o}$ is calculated by dividing this amount by the amount of Dox in the experimental solution, 10g/ml, to provide 8900 and 15,000 for 25◦C and 37◦C, respectively.

3.2. Simulation results

The model was solved numerically for an insonation period of 2s. Model parameters were determined by fitting the averaged experimental drug-release portion of the cycle. The experimental re-encapsulation portion of the cycle was compared to the predicted values. For each temperature, parameters for all three acoustic intensities were determined simultaneously. This method required that all data at a given temperature have the same values for the micelle re-assembly (˘) and re-encapsulation () parameters. The parameter for micelle destruction was allowed to vary as a function of acoustic intensity. Each parameter was determined by fitting a specific portion of the model to the release segment of the experimental data. The micelle destruction parameter (˛) was determined by the rapid initial rate of change in E. The difference in this parameter between the various acoustic intensities defined the difference in the minimum value attained for E throughout the cycle. The micelle re-encapsulation parameter () is determined by how quickly the rapid initial phase ceases. The micelle re-assembly parameter (˘) was determined using the data in the subsequent phase, at the point when E begins to plateau.

The model was able to simulate the drug release reasonably well, and to predict the subsequent drug re-encapsulation after ultrasound was turned off. The results of these simulations are presented in Figs. 3–5 for 25◦C, 37◦C, and 56◦C, respectively.

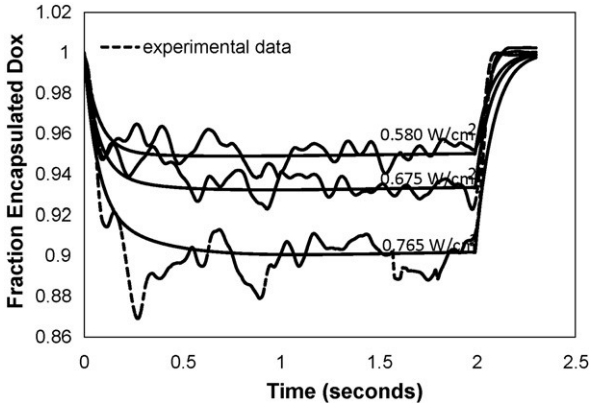

Fig. 4. Fluorescence data and model prediction at three different ultrasound intensities (0.580W/cm^2, 0.675W/cm^2 and 0.765W/cm^2) at 37◦C. Dotted line represents the average of 8 filtered runs. The solid line shows the fit of the model at the same temperature.

3.3. Thermodynamic analysis

The effect of temperature and acoustic intensity upon the model parameters can yield insight into thermodynamic characteristics of the mechanisms involved in micelle destruction, re-assembly, and drug encapsulation.

The parameter for destruction, ˛, depends on both the temperature and the acoustic intensity. The values for this parameter are shown in an Arrhenius plot in Fig. 6. For each acoustic intensity, the values of ˛ are well-described by an Arrhenius equation (displayed as a straight line on the figure). The slope of each line indicates the residual activation energy, or the amount of activation energy remaining for micelle destruction after it has been energized by ultrasound. The presence of ultrasound does not alter the energy barrier that must be surmounted for reaction to occur, but its contribution to the energy of the micelle decreases the residual amount of energy that must be provided thermally to cross the barrier. A similar system was proposed by Zhou et al. [52] in which ultrasound energized oxygen molecules and thereby partly overcame the energy barrier for oxygen activation and reaction. An analogous system can be found in photochemical reactions, where external energy from light energizes reactants and decreases the residual amount of energy required to cross the energy barrier for reaction to occur. This concept is illustrated in a schematic diagram using the reaction coordinate for micelle destruction (Fig. 7). Intact

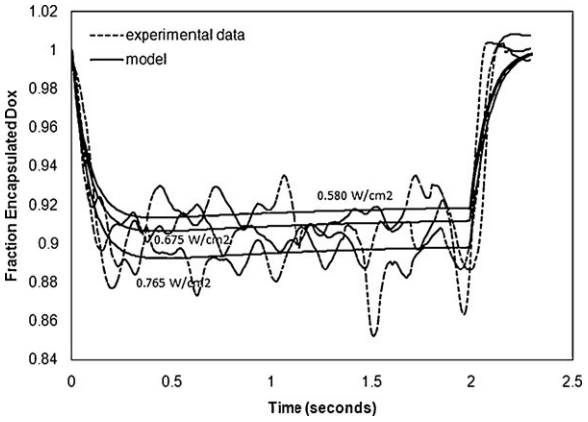

Fig. 5. Fluorescence data and model prediction at three different ultrasound intensities (0.580W/cm^2, 0.675W/cm^2 and 0.765W/cm^2) at 56◦C. Dotted line represents the average of 8 filtered runs. The solid line shows the fit of the model at the same temperature.

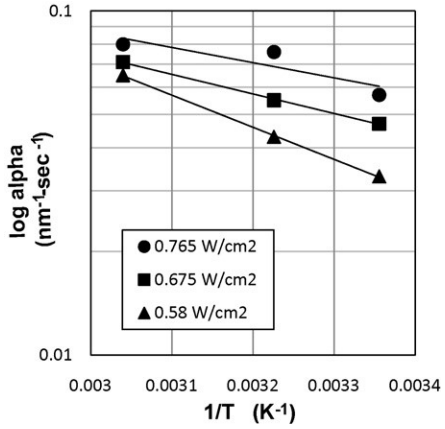

Fig. 6. The Arrhenius plot for ¸ (¸, the micellar destruction kinetic constant). The x-axis represents the reciprocal of the absolute temperature while the y-axis represents ¸ (log scale).

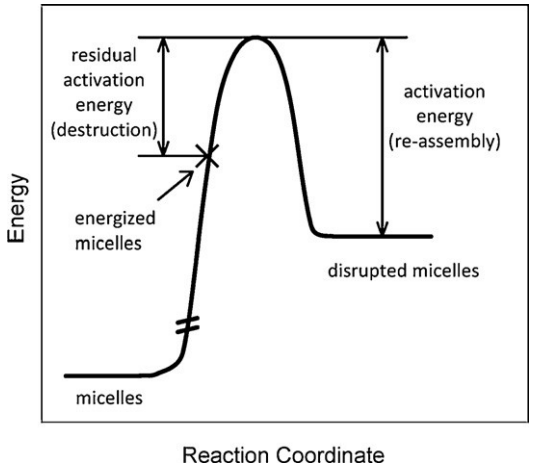

Fig. 7. Schematic diagram of the system energy vs reaction coordinate for micelle destruction.

micelles are on the left side of the figure, and disrupted micelles are on the right. Normally, micelles are at a relatively low energy, so that their destruction requires a large activation energy. Under insonation, the energy of micelles increases to a much higher level, and they become energized. This is denoted in Fig. 7. Once energized, micelles require much less additional energy to cross the energy barrier and become destroyed. The difference between the original activation energy and the amount of energy imparted to the micelle by the ultrasound is the residual activation energy. This residual activation energy can be found from the slope of an Arrhenius plot for each acoustic intensity.

Residual activation energies decrease with increasing acoustic intensity, as shown in Table 2. This is due to the increasing energy which the ultrasound imparts to the micelle, thus increasing the energy of an energized micelle, and decreasing the amount of residual energy required to destroy the micelle.

Table 2
Residual activation energies and correlation coefficients for ¸ (the micellar destruction kinetic constant) for three acoustic intensities.

Acoustic power (W/cm^2)	Residual activation energy (kJ/mol)	Correlation coefficient, R
0.58	18	>0.99
0.675	11	>0.99
0.765	8	0.88

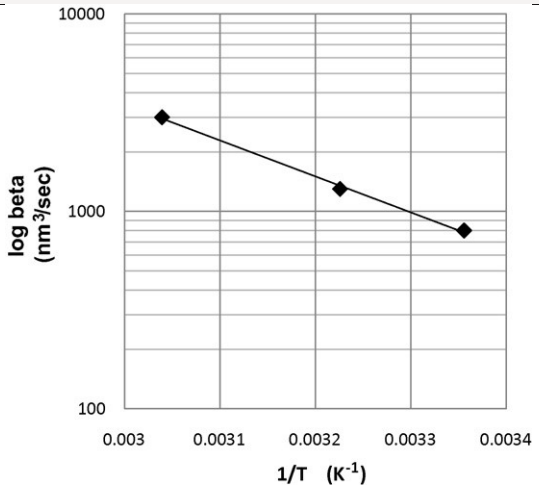

Fig. 8. The Arrhenius plot for ˇ (the micellar assembly kinetic constant). The x-axis represents the reciprocal of the absolute temperature while the y-axis represents ˇ (log scale).

The parameter for micelle re-assembly, ˇ, depends only on temperature. Its value increases rapidly with increasing

temperature, as is evident in the Arrhenius plot in Fig. 8. The observed values of ˇ are well-described by the Arrhenius equation, with a correlation coefficient of 0.99. The activation energy for micelle re-assembly can be calculated from the slope of this line. It was found to be 38kJ/mol.

The parameter for drug encapsulation by micelles, , is also only a function of temperature. Its value decreases slightly with increasing temperature; at 25◦C, 37◦C, and 56◦C, the values for were 255, 240, and 190m/s, respectively. This decrease with temperature is evident in the experimental data, since is related to how quickly the rapid initial phase of release ends. Stated differently, a brief initial phase dictates a large value of ; a longer initial phase dictates a smaller value of . At 25◦C and 37◦C, the end of the rapid initial phase, as observed in Figs. 3 and 4, occurs in the vicinity of 0.08s. At 56◦C, in Fig. 5, the end of the rapid initial phase occurs at approximately 0.15s, requiring a smaller value for at this temperature.

The decrease in with temperature indicates that the effective rate of encapsulation does likewise. This rate is the result of two mechanisms, encapsulation and diffusive release. The rate of the forward reaction, encapsulation increases with temperature, reflecting an increase in both the forward rate constant and the driving force, $^{E}_{tot}{}^{sat}_{,o}$. Similarly, the rate of the reverse reaction, diffusive release, also increases with temperature, due to an increase in both the rate constant and the driving force, or $[Dox]^{sat}_{PBS}$. Since the effective rate of encapsulation decreases slightly with temperature, then the rate of the reverse reaction must increase at a higher rate with temperature than that of the forward reaction. Nevertheless, at all temperatures studied, the forward reaction still predominates, as evidenced by a net positive rate of encapsulation.

The overall effect of temperature on micelle release can be observed by studying the minimum fraction of encapsulated Dox, E, for each temperature and acoustic intensity. Fig. 9 shows that the minimum value for E decreases with increasing temperature for each of the three acoustic intensities suggesting an increase in micelle destruction with temperature. This can be explained by a decrease in the viscosity of the solution surrounding the micelles as we increase the temperature. The lower viscosity is capable of decreasing the damping of bubble oscillations thus allowing collapse cavitation to occur at lower ultrasonic power densities. As a result, an increase in release percent is observed experimentally. We propose the mechanism illustrated in Fig. 7 to explain

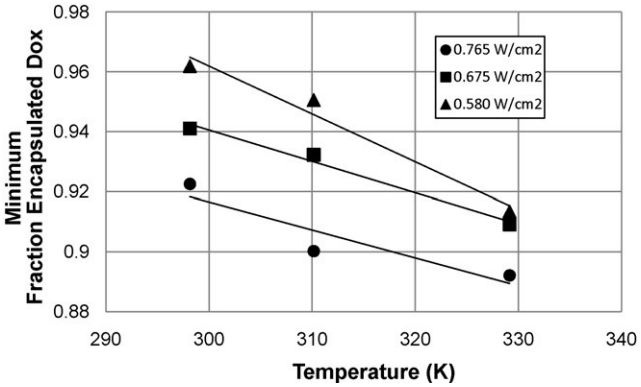

Fig. 9. Minimum fraction of encapsulated Dox as a function of temperature and acoustic intensity.

this phenomenon. An energized micelle can continue forward in the reaction to micelle destruction, or it may return to its normal state. Although both paths are exothermic, the one leading to micelle destruction is less so, and therefore will predominate as the temperature is increased.

3.4. Comparison to literature

In this paper, we reported the acoustic release and subsequent re-encapsulation kinetics and thermodynamics of Doxorubicin from Pluronic® P105 micelles. Several groups have studied the thermodynamic properties of polymeric micellization and assembly. Alexandridis et al. have studied Pluronic® properties in aqueous solutions [53–55]. His group found that the phase state of Pluronic® micelles can be controlled by choosing Pluronics with the appropriate molecular weight and PPO/PEO block length ratio, and by adjusting the concentration. The group extensively studied the thermodynamics of micellization of liquid (e.g. L64) paste (e.g. P105) and solid (e.g. F108) Pluronics [53]. They found that a closed association model was capable of adequately describing the thermodynamics of the micellization process. In these studies, they calculated the enthalpies (H◦), entropies (ΔS°) and Gibbs free energies (G◦) for several Pluronic® compounds and concluded that the self assembly process of micelle formation is entropy driven. Additionally, they reported that initial micellization is an endothermic process, i.e. they found the standard micellization enthalpy to be positive. To calculate the H◦, the slope of the reciprocal of the critical micellization concentration (T_{cmt}) vs ln(mole fraction) of each Pluronic® compound was determined, while to obtain the corresponding ΔG° for the same copolymer, Eq. (6) was used:

$$\Delta G^{o} = RT \ln(X_{cmc}) \quad (6)$$

where R is the universal gas constant, T is the temperature in K and X_{cms} is the critical micellization concentration (in mole fraction). The standard entropy was then calculated using the well known thermodynamic relationship:

$$\Delta S^o = \frac{\Delta H^o - \Delta G^o}{T}$$

Pluronic® P105 has a PPO/PEO fraction of 0.763 and an average molecular weight of 6500g/mol. Using the above equations, the group found that the standard enthalpy, Gibbs free energy and entropy of a 1% P105 solution were 331kJ/mol, −25.6kJ/mol and 1.212kJ/molK, respectively. The positive enthalpy suggests that individual P105 chains (or unimers) are more favored to accumulate in the micelle rather than stay in the surrounding aqueous solution. The negative free energy proves that micelle formation is a spontaneous process and the positive entropy indicate that when unimers accumulate in the form of a micelle the structure of the surrounding aqueous solution is restored (possibly due to the restoration of the hydrogen-bonding in the water surrounding the micelle) [53]. While Alexandridis et al. reported extensively on the thermodynamics of micelle formation, here we report on the thermodynamics of micelle destruction and assembly upon ultrasonication. The assembly or re-encapsulation of our system is also spontaneous and is entropy-driven. The release is a strong function of cavitation events which are highly correlated with acoustic intensity.

4. Conclusions

The kinetic and thermodynamic properties of ultrasonic release of drugs from unstabilized P105 micelles are reported herein. In a previous paper, we attempted the use of a mathematical model that accounts for cavitation events causing ultrasonic Dox release from micelles at 20kHz and 0.058W/cm^2. Here we extend the use of the model to study the kinetics of the same drug delivery system at three power densities and three temperatures using data obtained at 70-kHz US. The thermodynamics of the release phenomenon are then deduced using Arrhenius plots and the kinetic constants obtained at the three different temperatures. Our next step is to model drug-release dynamics from stabilized micelles and correlate these results with in vivo experiments.

Acknowledgments

The authors would like to acknowledge funding from the National Institutes of Health (R01 CA-98138) and the Faculty Research Grant at the American University of Sharjah (FRG-AUS08).

References

[1] G.A. Husseini, W.G. Pitt, Micelles and nanoparticles for ultrasonic drug and gene delivery, Advanced Drug Delivery Reviews 60 (10) (2008) 1137– 1152.

[2] D.N. Stephens, J. Cannata, R. Liu, J.Z. Zhao, K.K. Shung, H. Nguyen, R. Chia, A. Dentinger, D. Wildes, K.E. Thomenius, A. Mahajan, K. Shivkumar, K. Kim, M. O'Donnell, A. Nikoozadeh, O. Oralkan, P.T. Khuri-Yakub, D.J. Sahn, Multifunctionalcatheterscombiningintracardiacultrasoundimagingandelectrophysiology sensing, IEEE Transactions on Ultrasonics Ferroelectrics and Frequency Control 55 (7) (2008) 1570–1581.

[3] D.N. Stephens, J. Cannata, R.B. Liu, J.Z. Zhao, K.K. Shung, H. Nguyen, R. Chia, A. Dentinger, D. Wildes, K.E. Thomenius, A. Mahajan, K. Shivkumar, K. Kim, M. O'Donnell, D. Sahn, The acoustic lens design and in vivo use of a multifunctional catheter combining intracardiac ultrasound imaging and electrophysiology sensing, IEEE Transactions on Ultrasonics Ferroelectrics and Frequency Control 55 (3) (2008) 602–618.

[4] J.R. Wu, W.L. Nyborg, Ultrasound, cavitation bubbles and their interaction with cells, Advanced Drug Delivery Reviews accepted (2008).

[5] A.F.H. Lum, M.A. Borden, P.A. Dayton, D.E. Kruse, S.I. Simon, K.W. Ferrara, Ultrasound radiation force enables targeted deposition of model drug carriers loaded on microbubbles, Journal of Controlled Release 111 (1–2) (2006) 128– 134.

[6] P.A. Dayton, J.E. Chomas, A.F.H. Lum, J.S. Allen, J.R. lindner, S.I. Simon, K.W. Ferrara,Opticalandaccousticaldynamicsofmicrobubblecontrastagentsinside neutrophils, Biophysics Journal 80 (2001) 1547–1556.

[7] S.B. Stringham, M.A. Viskovska, E.S. Richardson, S. Ohmine, G.A. Husseini, B.K. Murray, W.G. Pitt, Over-pressure suppresses ultrasonic-induced drug uptake, Ultrasound in Medicine and Biology 35 (3) (2009) 409–415.

[8] G.A. Husseini, M.A. Diaz, E.S. Richardson, D.A. Christensen, W.G. Pitt, The role of cavitation in acoustically activated drug delivery, Journal of Controlled Release 107 (2) (2005) 253–261.

[9] M. Duvshani-Eshet, D. Adam, M. Machluf, The effects of albumin-coated microbubbles in DNA delivery mediated by therapeutic ultrasound, Journal of Controlled Release 112 (2) (2006) 156–166.

[10] R.K. Schlicher, H. Radhakrishna, T.P. Tolentino, R.P. Apkarian, V. Zarnitsyn, M.R. Prausnitz, Mechanism of intracellular delivery by acoustic cavitation, Ultrasound in Medicine and Biology 32 (6) (2006) 915–924.

[11] I.V. Larina, B.M. Evers, T.V. Ashitkov, C. Bartels, K.V. Larin, R.O. Esenaliev, Enhancement of drug delivery in

tumors by using interaction of nanoparticles with ultrasound radiation, Technology in Cancer Research & Treatment 4 (2) (2005) 217–226.

[12] I.V. Larina, B.M. Evers, R.O. Esenaliev, Optimal drug and gene delivery in cancer cells by ultrasound-induced cavitation, Anticancer Research 25 (1A) (2005) 149–156.

[13] W.G. Pitt, G.A. Husseini, B.J. Staples, Ultrasonic drug delivery—a general review, Expert Opinion in Drug Delivery 1 (1) (2004) 37–56.

[14] H. Ueda, M. Mutoh, T. Seki, D. Kobayashi, Y. Morimoto, Acoustic cavitation as an enhancing mechanism of low-frequency sonophoresis for transdermal drug delivery, Biological & Pharmaceutical Bulletin 32 (5) (2009) 916–920.

[15] M.M. Forbes, R.L. Steinberg, W.D. O'Brien, Examination of inertial cavitation of optison in producing sonoporation of Chinese hamster ovary cells, Ultrasound in Medicine and Biology 34 (12) (2008) 2009–2018.

[16] S. Hernot, A.L. Klibanov, Microbubbles in ultrasound-triggered drug and gene delivery, Advanced Drug Delivery Reviews 60 (10) (2008) 1153–1166.

[17] G.A. Husseini, N.Y. Rapoport, D.A. Christensen, J.D. Pruitt, W.G. Pitt, Kinetics of ultrasonic release of doxorubicin from Pluronic P105 micelles, Colloids and Surfaces B: Biointerfaces 24 (2002) 253–264.

[18] G.A. Husseini, G.D. Myrup, W.G. Pitt, D.A. Christensen, N.Y. Rapoport, Factors affecting acoustically-triggered release of drugs from polymeric micelles, Journal of Controlled Release 69 (2000) 43–52.

[19] A. Marin, H. Sun, G.A. Husseini, W.G. Pitt, D.A. Christensen, N.Y. Rapoport, Drug delivery in pluronic micelles: effect of high-frequency ultrasound on drug release from micelles and intracellular uptake, Journal of Controlled Release 84 (1) (2002) 39–47.

[20] G.A. Husseini, C.M. Runyan, W.G. Pitt, Investigating the mechanism of acoustically activated uptake of drugs from Pluronic micelles, BMC Cancer 2 (2002) 20.

[21] M.D.Muniruzzaman,A.Marin,Y.Luo,G.D.Prestwich,W.G.Pitt,G.Husseini,N.Y. Rapoport, Intracellular uptake of Pluronic copolymer: effects of the aggregation state, Colloids and Surfaces B: Biointerfaces 25 (3) (2002) 233–241.

[22] G.A. Husseini, M.A. Diaz de la Rosa, T. Gabuji, Y. Zeng, D.A. Christensen, W.G. Pitt, Release of doxorubicin from unstabilized and stabilized micelles under the action of ultrasound, Journal of Nanoscience and Nanotechnology 7 (3) (2007) 1–6.

[23] B.J. Staples, B.L. Roeder, G.A. Husseini, O. Badamjav, G.B. Schaalje, W.G. Pitt, Role of frequency and mechanical index in ultrasonic-enhanced chemotherapy in rats cancer, Chemotherapy and Pharmacology 64 (2009) 593–600.

[24] J.L. Nelson, B.L. Roeder, J.C. Carmen, F. Roloff, W.G. Pitt, Ultrasonically activated chemotherapeutic drug delivery in a rat model, Cancer Research 62 (2002) 7280–7283.

[25] N. Rapoport, W.G. Pitt, H. Sun, J.L. Nelson, Drug delivery in polymeric micelles:
from in vitro to in vivo, Journal of Controlled Release 91 (1–2) (2003) 85–95.

[26] G.A.Husseini,R.I.El-Fayoumi,K.L.O'Neill,N.Y.Rapoport,W.G.Pitt,DNAdamage induced by micellar-delivered doxorubicin and ultrasound: comet assay study, Cancer Letters 154 (2000) 211–216.

[27] G. Myhr, J. Moan, Synergistic and tumour selective effects of chemotherapy and ultrasound treatment, Cancer Letters 232 (2) (2006) 206–213.

[28] H. Hosseinkhani, T. Aoyama, S. Yamamoto, O. Ogawa, Y. Tabata, In vitro transfection of plasmid DNA by amine derivatives of gelatin accompanied with ultrasound irradiation, Pharmaceutical Research 19 (10) (2002) 1471–1479.

[29] H. Hosseinkhani, Y. Tabata, Ultrasound enhances in vivo tumor expression of plasmid DNA by PEG-introduced cationized dextran, Journal of Controlled Release 108 (2–3) (2005) 540–556.

[30] H. Hosseinkhani, Y. Inatsugu, Y. Hiraoka, S. Inoue, H. Shimokawa, Y. Tabata, Impregnation of plasmid DNA into three-dimensional scaffolds and medium perfusion enhance in vitro DNA expression of mesenchymal stem cells, Tissue Engineering 11 (9–10) (2005) 1459–1475.

[31] H. Hosseinkhani, T. Aoyama, O. Ogawa, Y. Tabata, Tumor targeting of plasmid DNA by dextran conjugation based on metal coordination, Asbm6: Advanced Biomaterials VI 288–289 (2005) 109–112.

[32] H. Hosseinkhani, Y. Tabata, PEGylation enhances tumor targeting of plasmid DNA by an artificial cationized protein with repeated RGD sequences, Pronectin((R)), Journal of Controlled Release 97 (1) (2004) 157–171.

[33] H. Hosseinkhani, T. Azzam, Y. Tabata, A.J. Domb, Dextran-spermine polycation: an efficient nonviral vector for in vitro and in vivo gene transfection, Gene Therapy 11 (2) (2004) 194–203.

[34] H. Hosseinkhani, DNA nanoparticles for gene delivery to cells and tissue, International Journal of Nanotechnology 3 (4) (2006) 416–461.

[35] H. Hosseinkhani, Y. Tabata, Self assembly of DNA nanoparticles with polycations for the delivery of genetic materials into cells, Journal of Nanoscience and Nanotechnology 6 (8) (2006) 2320–2328.

[36] D. Stevenson-Abouelnasr, G.A. Husseini, W.G. Pitt, Further investigation of the mechanism of Doxorubicin release from P105 micelles using kinetic models, Colloids and Surfaces B: Biointerfaces 55 (1) (2007) 59–66.

[37] V. Sboros, Response of contrast agents to ultrasound, Advanced Drug Delivery Reviews 60 (10) (2008) 1117–1136.

[38] M. Ashokkumar, J. Lee, Y. Iida, K. Yasui, T. Kozuka, T. Tuziuti, A. Towata, The detection and control of stable and transient acoustic cavitation bubbles, Physical Chemistry Chemical Physics 11 (43) (2009) 10118–10121.

[39] K. Yasui, J. Lee, T. Tuziuti, A. Towata, T. Kozuka, Y. Lida, Influence of the bubble-bubble interaction on destruction of encapsulated microbubbles under ultrasound, Journal of the Acoustical Society of America 126 (3) (2009) 973–982.

[40] E. Biagi, L. Breschi, E. Vannacci, L. Masotti, Stable and transient subharmonic emissions from isolated contrast agent microbubbles, IEEE Transactions on Ultrasonics Ferroelectrics and Frequency Control 54 (3) (2007) 480–497.

[41] S. Casciaro, R.P. Errico, F. Conversano, C. Demitri, A. Distante, Experimental investigations of nonlinearities and destruction mechanisms of an experimental phospholipid-based ultrasound contrast agent, Investigative Radiology 42 (2) (2007) 95–104.

[42] Z. Sun, X.Q. Kang, X.H. Wang, Experimental system of cavitation erosion with water-jet, Materials & Design 26 (1) (2005) 59–63.

[43] E.S. Richardson, W.G. Pitt, D.J. Woodbury, The role of cavitation in liposome formation, Biophysical Journal 93 (12) (2007) 4100–4107.

[44] G. Enden, A. Schroeder, A mathematical model of the controlled release of drugs from liposomes y low-frequency ultrasound, Annuls of Biomedical Engineering 37 (12) (2009) 2640–2645.

[45] H.Y. Lin, J.L. Thomas, Factors affecting responsivity of unilamellar liposomes to 20kHz ultrasound, Langmuir 20 (15) (2004) 6100–6106.

[46] N.B. Smith, Perspectives on transdermal ultrasound mediated drug delivery, International Journal of Nanomedicine 2 (4) (2007) 585–594.

[47] K.W. Ferrara, M.A. Borden, H. Zhang, Lipid-shelled vehicles: engineering for ultrasound molecular imaging and drug delivery, Accounts of Chemical Research 42 (7) (2009) 881–892.

[48] J.A. Kopechek, T.M. Abruzzo, B. Wang, S.M. Chrzanowski, D.A.B. Smith, P.H. Kee, S. Huang, J.H. Collier, D.D. McPherson, C.K. Holland, Ultrasound-mediated release of hydrophilic and lipophilic agents from echogenic liposomes, Journal of Ultrasound in Medicine 27 (11) (2008) 1597–1606.

[49] S.L. Huang, Liposomes in ultrasonic drug and gene delivery, Advanced Drug Delivery Reviews 60 (10) (2008) 1167–1176.

[50] D.A.B. Smith, T.M. Porter, J. Martinez, S.L. Huang, R.C. MacDonald, D.D. McPherson, C.K. Holland, Destruction thresholds of echogenic liposomes with clinical diagnostic ultrasound, Ultrasound in Medicine and Biology 33 (5) (2007) 797–809.

[51] J. Pruitt, Stabilization of Pluronic P-105 for Targeted Nanoparticle Drug Delivery, Chemical Engineering Department, Brigham Young University, Provo, 2001.

[52] T. Zhou, T.T. Lim, Y. Li, X. Lu, F.S. Wong, The role and fate of EDTA in ultrasoundenhanced zero-valent iron/air system, Chemosphere 78 (2010) 576–582.

[53] P. Alexandridis, J.F. Holzwarth, T.A. Hatton, Micellization of poly(ethylene oxide)-poly(propylene oxide)-poly(ethylene oxide) triblock copolymer in aqueous solutions: thermodynamics of copolymer association, Macromolecules 27 (9) (1994) 2414–2425.

[54] P. Alexandridis, T. Nivaggioli, T.A. Hatton, Temperature effects on structural properties of Pluronic P104 and F108 PEO-PPO-PEO block copolymer solutions, Langmuir 11 (1995) 1468–1476.

[55] P. Alexandridis, V. Athanassiou, T.A. Hatton, Pluronic-P105 PEO-PPO-PEO block copolymer in aqueous urea solutions: micelle formation. structure, and microenvironment, Langmuir 11 (1995) 2442–2450.